Indian Journal of Pure & Applied Physics
Vol. 58, March 2020, pp. 178-188

Effect of buoyancy and suction on Sisko nanofluid over a vertical stretching sheet in a porous medium with mass flux condition

Rajesh Sharma* & Ankita Bisht

Department of Mathematics and Scientific Computing, National Institute of Technology, Hamirpur 177 005, India

Received 17 November 2018; accepted 10 January 2020

The present article investigates the flow and heat transfer of Sisko nanofluid over a permeable vertical stretching surface in a porous medium. The effect of buoyancy, suction, and viscous dissipation has been taken into account. Buongiorno's model of nanofluid consisting of thermophoresis and Brownian diffusion has been considered. Moreover, zero nanoparticle mass flux condition is employed at the boundary which leads to a more realistic physical problem. Using a suitable transformation governing partial differential equations of fluid flow are transformed into a set of nonlinear ordinary differential equations (ODEs). The numerical solution of nonlinear ODEs are obtained using the finite difference technique in MATLAB. The influence of physical parameters viz. buoyancy parameter (λ^*), porosity parameter (β^*), thermophoresis parameter (Nt^*), suction parameter (f_w^*), Sisko material parameter (A^*), Brinkman number (Br^*), Brownian diffusion parameter (Nb^*) and Lewis number (Le^*) on velocity, temperature and nanoparticle volume fraction are shown graphically. Moreover, to understand the physical phenomenon in the boundary layer region, the numerical values of skin friction and Nusselt number are calculated and presented through table values. It has been found that the Brownian diffusion has a negligible impact on Nusselt number relative to the results obtained in previous studies, where nanoparticle volume fraction on the boundary was actively controlled. The obtained results disclose that the buoyancy parameter increases the velocity of fluid while it reduces the temperature. Suction parameter reduces both velocity and temperature, whereas the porosity parameter reduces velocity and enhances the temperature and nanoparticle volume fraction.

Keywords: Sisko nanofluid, Buoyancy effect, Suction, Viscous dissipation, Porous medium, Nanoparticles mass flux condition

1 Introduction

The flow over a stretching sheet has gained considerable attention due to its important role in the production of polymers, aerospace applications, metal casting and thus remains at the leading edge of technology development. In view of such applications, Crane[1] initiated the analytical study of boundary layer flow of viscous fluid due to the stretching of an elastic sheet in its own plane. He assumed linearly varying velocity along the distance from a fixed point due to the uniform stress. Later on, many researchers[2-4] extended the work of Crane by assuming different physical conditions on flow, heat and mass transfer.

The concept of boundary layer flow has gained considerable importance due to its vast applications in the calculation of the skin-friction drag, such as the drag of a ship or of an airplane wing, the drag experienced by a flat plate at zero incidence, turbine blade or aircraft nacelle, etc. The problems of heat and mass transfer between a flowing fluid and a solid body also belong to the class where boundary layer phenomenon plays a key role. In the regions of an adverse pressure gradient or in case of steep pressure curves, boundary layer separation occurs. Suction is an effective method for the prevention of separation in the boundary layer. It removes the deaccelerated fluid particles from the boundary layer before they cause separation. Moreover, owing to the absence of separation the amount of pressure drag is greatly reduced. Suction is successfully used in airplane wings to increase the lift and in recent times it is applied to reduce drag. Some studies dealing with the effect of suction on flow and heat transfer are mentioned in Gupta and Gupta[5], Reddy and Sidawi[6], Gupta *et al.*[7], etc.

In the heat transfer process of many practical problems, viscous dissipation plays an important role. The heat generated due to viscous dissipation increases temperature near the wall. Brinkman[8] was first, who investigated the heat transfer in fluid flow and analyzed the temperature distribution in a capillary, due to heat

*Corresponding author (E-mail: raj.juit@gmail.com)

dissipation. A mathematical model of viscous dissipation within a fluid-saturated porous medium has been studied by several researchers[9-11] in different ways. For the viscous dissipation effect in Darcy medium, they have included only one term with the velocity derivative, which is found to be infeasible in many practical cases. Al-Hadhrami *et al.*[12] proposed a more appropriate model for viscous dissipation in a porous medium. Later on, Sharma[13] modeled the viscous dissipation effect, according to Al-Hadhrami *et al.* and obtained an approximate numerical solution using EFGM.

The problem of mixed convection flow has been studied by many authors[14-17] due to its practical importance in engineering processes such as petroleum extraction, in the storage of agricultural products, as a porous material heat exchanger, flows in the ocean and atmosphere, drying of porous solids, nuclear reactors, atmospheric boundary layer flows, solar collectors, etc. In many practical convection, the hydrodynamic and thermal boundary layer is affected by buoyancy forces due to heating or cooling of the stretching surface. Hayat *et al.*[18] studied the characteristics of mixed convection in Burger nanofluid flow in the presence of both concentration and thermal stratification. Waqas *et al.*[19] investigated the mixed convective flow of Jeffrey fluid over a moving stratified surface. Waqas *et al.*[20] obtained the analytical solution of MHD flow of micropolar liquid due to a stretching surface using the Homotopic procedure. Waqas *et al.*[21] studied the transport of radiative energy in viscoelastic nanofluid, taking into account convective conditions and buoyancy forces.

In the fastest growing technology, the flow and heat transfer analysis of nanofluids has been given much attention due to its particular applications in solar water heating, domestic refrigerator-freezers, improving diesel generator efficiency, in a nuclear reactor, cooling of machines, transformer, and engines, etc. The term nanofluid refers to the fluid with enhanced thermal conductivity, formed by suspending nanoparticles in the base fluid and has been introduced by Choi[22]. In recent years, various researchers[23-28] have elucidated the nanofluid flow and heat transfer by considering various physical aspects.

In modern engineering applications and industrial processes, the role of heat and mass transfer is quite important. In addition to traditional research in internal combustion engines, power plants, air conditioning, and refrigeration, cutting-edge research such as additive manufacturing, thermal management, and nano transport phenomena in biological systems has become prominent. In various applications such as diesel-electric conductor, solar thermal collector, electronic equipment, and nuclear reactor ongoing research in complex nanofluid has been fruitful. A substantial amount of nanoparticles serves for deeper absorption of incident radiation and thus improves the solar thermal collector's performance[29,30].

All of the above-mentioned studies are restricted to Newtonian fluids. However, due to wide occurrence and enormous practical utility of non-Newtonian fluids in industrial and biological sectors including polymer, plastic, food, mineral suspensions, pharmaceutical, cosmetics, personal care products, construction materials, etc. flow and heat transfer analysis of non-Newtonian fluids has become the main area of research nowadays. Hayat *et al.*[31] studied the double stratified flow of Oldroyd-B liquid with chemical reaction and examined the heat transfer characteristics using the non-Fourier heat flux model. Eid *et al.*[32] proposed Carreau nanofluid flow over a porous nonlinear stretching surface. Recently, Bisht and Sharma[33] obtained the non-similar solution of casson nanofluid with variable thermal conductivity and viscosity. Waqas[34] analyzed the ferromagnetic williamson fluid flow considering magnetic dipole and found that temperature and velocity fields have reverse conduct for the ferrohydrodynamic interaction parameter. So, it is observed from the available literature that several mathematical models have been proposed to describe the non-Newtonian fluids present in nature, among which one is Sisko model[35]. Sisko fluid model was initially proposed for the measurements of high shear rates on lubricating grease. Further, it can be effectively used for non-Newtonian fluids over a wide range of shear stresses. This model is good at predicting the shear thinning and shear thickening behavior of the fluid. It is a three-parameter model which is basically a generalization of both viscous and power-law fluid models.

The flow and heat transfer over a stretching surface in porous media is an important phenomenon in many disciplines of science and engineering. The most common examples include chemical reactors, hydrology, geophysics, groundwater flow, heat exchange systems, insulation engineering, and oil recovery processes. Moreover, the magnetic effect and porous medium are often used to control the transport phenomenon in electrically conducting media. Eid and Mahny[36] investigated the flow and heat transfer of Sisko nanofluid saturated porous

medium with heat absorption/ generation. Doh *et al.*[37] used the Cattaneo-Christov heat flux model to study the three dimensional Sisko fluid flow through a porous medium. Soomro *et al.*[38] investigated the Sisko nanofluid flow, heat and mass transfer subjected to the transverse magnetic field and thermal radiation. Ahmad and Khan[39] portrayed the influence of chemical reaction and activation energy on the MHD Sisko nanofluid through a porous curved surface. Sharma and Bisht[40] investigated the impact of Joule heating on heat transfer and flow of the Sisko nanofluid. Recently, Asghar *et al.*[41] presented the first theoretical model that analyses the mass and heat transfer impacts on peristaltic flow generated due to the wavy walls in a porous curved channel.

To the best of authors knowledge flow and heat transfer of Sisko nanofluid over a vertical stretching sheet with viscous dissipation effect in a porous medium has not been given due attention. So, we fill the gap in the literature by investigating the effect of buoyancy and viscous dissipation on the flow and heat transfer of Sisko nanofluid over a permeable vertical stretching sheet dipped in a porous medium. In this article, viscous dissipation effect is modeled according to Al-Hadhrami *et al.*[12] and a zero nanoparticle mass flux condition at the boundary is considered according to Kuznetsov and Nield[42]. The numerical results of the skin friction, Nusselt number, velocity, temperature, and nanoparticle volume fraction for different physical parameters are presented through tables and graphs.

2 Mathematical Model

Consider a 2-D, steady flow of Sisko nanofluid along a vertical permeable stretching sheet embedded in a porous medium in the presence of a magnetic field and viscous dissipation effects. The y-axis is taken as a horizontal plane and the x-axis is vertical to it. The flow is restricted in the $y > 0$ region. The fluid motion arises due to continuous stretching surface velocity $U_w = cx^{s^*}$, where $s^* > 0$ denotes the stretching rate of the sheet and c denotes a positive real number. A physical model and coordinate system are sketched in Fig. 1. The magnetic field of strength B_0 is imposed on the fluid particles in the direction perpendicular to the x-axis and it is sufficiently weak to ignore hall effects and induction. The nanoparticle volume fraction is passively controlled by employing zero nanoparticle mass flux condition at the boundary. The stretching sheet is in contact with hot fluid with temperature T_w. The flux of the nanoparticle volume

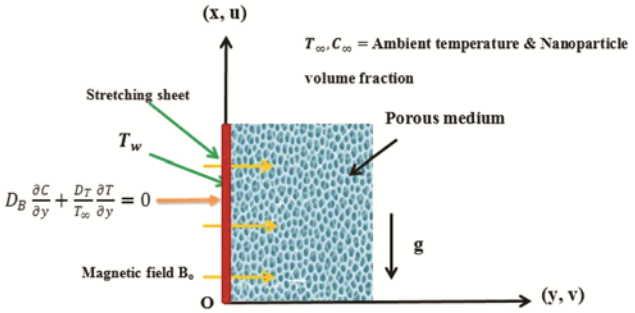

Fig. 1 — Flow model and coordinate system.

fraction at $y = 0$ is taken to be zero. Temperature and nanoparticle volume fraction in the free stream is taken as constant, i.e., T_∞ and C_∞.

On the basis of Boussinesq and boundary layer approximation, the governing equation of flow in two dimensions are as follows[36]:

$$\frac{\partial u}{\partial x} + \frac{\partial v}{\partial y} = 0 \quad \ldots (1)$$

$$u\frac{\partial u}{\partial x} + v\frac{\partial u}{\partial y} = \frac{a^*}{\rho_{nf}}\frac{\partial^2 u}{\partial y^2} - \frac{b^*}{\rho_{nf}}\frac{\partial}{\partial y}\left(-\frac{\partial u}{\partial y}\right)^{n^*} - \frac{\sigma B_0^2 u}{\rho_{nf}} - \frac{\mu\varepsilon}{\rho_{nf}K_p^*}u + g(T - T_\infty)\beta_t + g(C - C_\infty)\beta_c \quad \ldots (2)$$

$$u\frac{\partial T}{\partial x} + v\frac{\partial T}{\partial y} = \frac{1}{(\rho C)_{nf}}\frac{\partial}{\partial y}\left(\alpha\frac{\partial T}{\partial y}\right) + \frac{\sigma}{(\rho C)_{nf}}B_0^2 u^2 + \frac{1}{(\rho C)_{nf}}\left[\frac{\mu\varepsilon}{K_p^*}u^2 + a^*\left(-\frac{\partial u}{\partial y}\right)^2 + b^*\left(-\frac{\partial u}{\partial y}\right)^{n^*+1}\right] + \tau\left[D_B\frac{\partial C}{\partial y}\frac{\partial T}{\partial y} + \frac{D_T}{T_\infty}\left(\frac{\partial T}{\partial y}\right)^2\right] \quad \ldots (3)$$

$$u\frac{\partial C}{\partial x} + v\frac{\partial C}{\partial y} = D_B\frac{\partial^2 C}{\partial y^2} + \frac{D_T}{T_\infty}\frac{\partial^2 T}{\partial y^2} \quad \ldots (4)$$

and associated boundary conditions are:

$$\text{At y} = 0: u = U_w = cx^{s^*}, v = v_w, \quad T = T_w,\ D_B\frac{\partial C}{\partial y} + \frac{D_T}{T_\infty}\frac{\partial T}{\partial y} = 0$$

$$\text{and as y} \to \infty: u \to 0, T \to T_\infty, C \to C_\infty \quad \ldots (5)$$

Where, velocity components of the fluid in (x, y) direction are (u, v), $n^*(\geq 0)$ is power-law index, a^* and b^* are material constants for Sisko fluid, B_0 is the magnitude of the applied magnetic field. α, κ and K_p^* are the thermal diffusivity, thermal conductivity, and permeability of the porous medium, ρ_{nf} is the nanofluid density, σ is the electrical conductivity, D_T and D_B denotes the thermophoresis diffusion

coefficient and the Brownian diffusion coefficient, respectively. β_t denotes the coefficient of thermal expansion, v_w is mass flux velocity ($v_w > 0$ denotes suction and $v_w < 0$ denotes injection), $\tau = \frac{(\rho C)_{np}}{(\rho C)_{nf}}$ represent the ratio of the effective heat capacity of the nanoparticle to the heat capacity of nanofluid.

In Eq. (5), statement $D_B \frac{\partial C}{\partial y} + \frac{D_T}{T_\infty}\frac{\partial T}{\partial y} = 0$ ensures that at the boundary with thermophoresis taken into account, the normal flux of nanoparticles is zero (Kuznetsov and Nield[42]).

Following similarity transformations are introduced:

$$\eta = \frac{y}{x} Re_{b^*}^{\frac{1}{n^*+1}}, \varsigma(x,y) = xU_w Re_{b^*}^{-\frac{1}{n^*+1}} f(\eta),$$
$$\theta = \frac{T-T_\infty}{T_w-T_\infty}, \phi = \frac{C-C_\infty}{C_w} \quad \ldots (6)$$

Where, $Re_{b^*} = \frac{\rho_f x^{n^*} U_w^{2-n^*}}{b^*}$ is modified Reynolds number and $\varsigma(x,y)$ is the stream function defined as:

$$\mathrm{u} = \frac{\partial \varsigma}{\partial \mathrm{y}} \text{ and } \mathrm{v} = -\frac{\partial \varsigma}{\partial \mathrm{x}} \quad \ldots (7)$$

Using Eqs (6 and 7), Eqs (2-5) thereby reduces to the following nonlinear coupled ordinary differential equations:

$$n^*(-f'')^{n^*-1} f''' + A^* f''' + \left(\frac{s^*(2n^*-1)+1}{n^*+1}\right) f f'' - s^* f'^2 - M^* f' - \beta^* f' + \lambda^* \theta + Nr^* \phi = 0 \quad \ldots (8)$$

$$\theta'' + Br^*[A^*(-f'')^2 + (-f'')^{n^*+1} + \beta^* f'^2 + M^* f'^2] + Nt^* \theta'^2 + Nb^* \theta' \phi' + Pr^* \left(\frac{s^*(2n^*-1)+1}{n^*+1}\right) f\theta' = 0 \cdots \quad \ldots (9)$$

$$\phi'' + \frac{Nt^*}{Nb^*}\theta'' + Le^* Pr^* \left(\frac{s^*(2n^*-1)+1}{n^*+1}\right) f\phi' = 0 \quad \ldots (10)$$

and the transformed boundary conditions are:

$$f(0) = f_w^*, f'(0) = 1, \theta(0) = 1, \quad Nb^* \phi'(0) + Nt^* \theta'(0) = 0$$

$$\text{As } \eta \to \infty, f'(\eta) \to 0, \theta(\eta) \to 0, \phi(\eta) \to 0 \quad \ldots (11)$$

Where, the prime denotes differentiation with respect to η. The fluid regime is completely governed by physical parameters viz. Sisko material parameter A^*, suction parameter f_w^* ($f_w^* > 0$ suction and $f_w^* < 0$ injection), Eckert number Ec^*, modified Prandtl number Pr^*, magnetic parameter M^*, Brinkman number Br^*, thermophoresis parameter Nt^*, modified Reynold's number (Re_{b^*} and Re_{a^*}), Brownian diffusion parameter Nb^*, buoyancy ratio parameter Nr^*, porosity parameter β^*, Lewis number Le^*, thermal Grashoff number Gr^* and buoyancy parameter λ^*. The mixed convection flow is measured by the buoyancy parameter λ^* (where $\lambda^* >> 1$ implies forced convection may be ignored, $\lambda^* \approx 1$ combined forced and free convection, $\lambda^* << 1$ implies free convection may be neglected).

$$A^* = \frac{Re_{b^*}^{2/(n^*+1)}}{Re_{a^*}}, Ec^* = \frac{U_w^2}{C_{nf}(T_w - T_\infty)},$$

$$M^* = \frac{\sigma B_0^2 x}{\rho_{nf} U_w}, Br^* = Ec^* Pr^*, Nb^* = \frac{\tau D_B C_\infty}{\alpha}, f_w^* = \frac{v_w\,(n+1)}{U_w\,(s^*(2n-1)+1)} Re_{b^*}^{\frac{1}{n+1}}, Pr^* = \frac{xU_w}{\alpha} Re_{b^*}^{-2/(n^*+1)}, Nt^* = \frac{\tau D_T (T_w - T_\infty)}{\alpha T_\infty},$$

$$Le^* = \frac{\alpha}{D_B}, Re_{b^*} = \frac{\rho_{nf} x^{n^*} U_w^{2-n^*}}{b^*}, \beta^* = \frac{\nu \varepsilon x}{K_p^* U_w},$$
$$Gr^* = \frac{g\beta_t (T_w - T_\infty) x^3 \rho_{nf}^2}{a^{*2}}, Re_{a^*} = \frac{\rho_f U_w x}{a^*}, Nr^* = \frac{\beta_c C_\infty}{\beta_t (T_w - T_\infty)}, \lambda^* = \frac{Gr^*}{Re_{a^*}^2}$$

3 Physical Quantities of Interest

The important boundary layer characteristic, i.e., skin friction (dimensionless shear stress at the wall) and local Nusselt number (the heat transfer rate at the wall) is given by the following expressions, respectively:

$$C_{fx} = \frac{2\tau_{xy}}{\rho_{nf} U_w^2} \quad \ldots (12)$$

$$Nu_x = \frac{x q_w}{\kappa\,(T_w - T_\infty)} \quad \ldots (13)$$

Where,

$$\tau_{xy} = \left[a^* \frac{\partial u}{\partial y} - b^* \left(-\frac{\partial u}{\partial y}\right)^{n^*-1} \frac{\partial u}{\partial y}\right]\Bigg|_{y=0} \quad \ldots (14)$$

$$q_w = -\kappa \frac{\partial T}{\partial y}\Big|_{y=0} \quad \ldots (15)$$

Now using Eqs (6 and 7) the aforementioned relations in the non-dimensional form can be given as:

$$\frac{1}{2}C_{fx}Re_{b^*}^{1/(n^*+1)} = A^* f''(0) - (-f''(0))^{n^*} \quad \ldots (16)$$

$$Re_{b^*}^{-1/(n^*+1)}Nu_x = -\theta'(0) \quad \ldots (17)$$

We must note that dimensionless mass flux, i.e., Sherwood number Sh_x is identically zero here.

4 Numerical Solutions

The nonlinear coupled ordinary differential Eqs (8–11) are converted into a system of first-order ODEs with associated boundary conditions using new variables. Numerical solutions are obtained using a finite difference method in MATLAB. It is a finite difference code that uses a collocation method which is fourth-order accurate. The relative error tolerance is set to 0.5×10^{-10} . To solve these equations it is assumed that:

$$f = z_1, f' = z_2, f'' = z_3,$$

$$f''' = -\frac{1}{(n^*(-z_3)^{n^*-1}+A^*)}\left[-s^* {z_2}^2 - M^* z_2 + \left(\frac{s^*(2n^*-1)+1}{n^*+1}\right) z_1 z_3 - \beta^* z_2 + \lambda^* z_4 + Nr^* z_6\right]$$

$$\theta = z_4, \theta' = z_5$$

$$\theta'' = -\left[Br^*(A^* {z_3}^2 + (-z_3)^{n^*+1} + \beta^* {z_2}^2 + M^* {z_2}^2) + Nt^* {z_5}^2 + Nb^* z_5 z_7 + Pr^*\left(\frac{s^*(2n^*-1)+1}{n^*+1}\right) z_1 z_5\right]$$

$$\phi = z_6, \phi' = z_7,$$

$$\phi'' = -\frac{Nt^*}{Nb^*} z_5' Le^* Pr^*\left(\frac{s^*(2n^*-1)+1}{n^*+1}\right) z_1 z_7$$

with the following boundary conditions:

$$z_1(0) = f_w^*,\ z_2(0) = 1, z_4(0) = 1$$

$$Nb^* z_7(0) + Nt^* z_5(0) = 0,$$

$$z_2(\eta_\infty) = 0, z_4(\eta_\infty) = 0, z_6(\eta_\infty) = 0$$

For the computational purpose and without the loss of generality η_∞ (the edge of the boundary) has been fixed as 8. If η_∞ is taken to be more than 8, there is no significant change in the values of velocity, temperature and nanoparticle volume fraction upto the desired order of accuracy 0.5×10^{-10} as given via. Table 1.

5 Validation of the Code

To validate our finite difference code, a comparison of the present result for Nusselt number is done with the published work of Wang[43] and is shown in Table 2. This computation is carried out by assuming ($A^* = M^* = \beta^* = Ec^* = \lambda^* = Nt^*$ =0, $Nb^* \to 0$ and $Le^* = 1$, $s^* = 1$, $n^* = 1$) and it shows good agreement with the results obtained by Wang[43].

6 Results and Discussion

The velocity $f'(\eta)$, temperature $\theta(\eta)$, skin friction and nanoparticle volume fraction $\phi(\eta)$ for different physical parameters viz. Sisko material parameter A^*, suction parameter f_w^*, porosity parameter β^*, thermophoresis parameter Nt^*, buoyancy parameter λ^*, Brinkman number Br^*, Brownian diffusion parameter Nb^*, Lewis number Le^* are shown via Figs 2-17 for both shear thickening (n^* 1) and shear thinning ($0 < n^* < 1$) fluids. Impact of physical

Table 2 — A comparison of local Nusselt number $-\boldsymbol{\theta'(0)}$ for different values of $\boldsymbol{Pr^*}$.

Pr^*	$-\theta'(0)$(Present)	$-\theta'(0)$Wang[43]
0.7	0.45404	0.4539
2	0.91135	0.9114
7	1.89540	1.8954
20	3.35389	3.3539
70	6.46219	6.4622

Table 1 — Values of velocity, temperature and nanoparticle volume fraction for different η_∞.

	η_∞								
	Velocity			Temperature			Nanoparticle volume fraction		
η	6	8	10	6	8	10	6	8	10
1	0.30212	0.30213	0.30213	0.37567	0.37576	0.37576	0.17804	0.17814	0.17814
2	0.05466	0.05468	0.05468	0.08689	0.08701	0.08701	0.07059	0.07071	0.07071
3	0.00675	0.00677	0.00677	0.01736	0.01749	0.01749	0.01641	0.01654	0.01654
4	0.00085	0.00087	0.00087	0.00329	0.00342	0.00342	0.00324	0.00337	0.00337
5	0.00011	0.00013	0.00013	0.00053	0.00066	0.00066	0.00053	0.00066	0.00066

parameters β^* and f_w^* on skin friction and the heat transfer rate is given via. Tables 3 and 4. Table 5 represents the independency of the Nusselt number with the Brownian diffusion parameter due to the involvement of zero mass flux condition at the wall.

Skin friction reduces with increase in β^* and f_w^* as given in Table 3. The negative sign of skin friction coefficient implies that the drag force is exerted by stretching sheet on the fluid. Suction is applied to reduce the drag and stabilize the boundary layer[44]. Hence, skin friction reduces with increasing values of the suction parameter f_w^* and porosity parameter β^*.

The rate of heat transfer is governed by $-\theta'(0)$. Positive values of $(-\theta'(0))$ imply that heat is transferring from plate to the fluid. Heat transfer rate reduces with increase in β^* while a reverse trend is observed for f_w^* as mentioned in Table 4. Hence, suction can be effectively used in many industrial processes to control the temperature.

Table 5 shows the numerical values of Nusselt number or heat transfer rate $(-\theta'(0))$ for different values of Nt^* and Nb^*.The numerical result reveals that Nusselt number is a decreasing function of thermophoresis parameter Nt^* while it is independent of Brownian diffusion parameter Nb^* since the nanoparticle flux at the boundary is taken as zero. This result coincides with the explanation given by Kuznetsov and Nield[42]. Due to this zero mass flux condition at the boundary, Brownian motion's contribution to the energy equation which is proportional to the nanoparticle volume fraction gradient becomes zero as the wall is approached.

The impact of physical parameters A^*, β^*, λ^*, and f_w^* on velocity profile $f'(\eta)$ is given in Figs 2-5.

Figure 2 shows the effect of the Sisko material parameter A^* on velocity. A^* has an inverse relationship with the viscosity of the fluid in the power-law region, (i.e., consistency index b^*). So, when A^* increases viscous forces become weaker, thus less resistance is offered to the fluid motion.

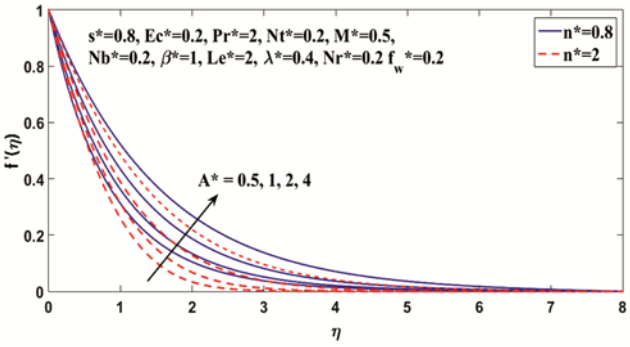

Fig. 2 — Behaviour of $\boldsymbol{f'(\eta)}$ with $\boldsymbol{A^*}$ against $\boldsymbol{\eta}$.

Table 3 — Skin friction for various values of porosity parameter β^* and suction f_w^*.

	$f_w^* = 0$		$f_w^* = 0.5$		$f_w^* = 1$		$f_w^* = 2$	
β^*	n^*=0.8	n^*=2	n^*=0.8	n^*=2	n^*=0.8	n^*=2	n^*=0.8	n^*=2
0	-1.24424	-1.10548	-1.48937	-1.51983	-1.75729	-1.97355	-2.35291	-2.95206
0.5	-1.48434	-1.35658	-1.72872	-1.76654	-1.99134	-2.20858	-2.56717	-3.15936
1	-1.69307	-1.58766	-1.93596	-1.99430	-2.19430	-2.42770	-2.75568	-3.35665
1.5	-1.87967	-1.80349	-2.12094	-2.20748	-2.37573	-2.63419	-2.92586	-3.54546
2	-2.04971	-2.00723	-2.28933	-2.40900	-2.54109	-2.83034	-3.08210	-3.72696

Table 4 — Heat transfer rate $-\theta'(0)$ for various values of porosity parameter β^* and suction f_w^*.

	$f_w^* = 0$		$f_w^* = 0.5$		$f_w^* = 1$		$f_w^* = 2$	
β^*	n^*=0.8	n^*=2	n^*=0.8	n^*=2	n^*=0.8	n^*=2	n^*=0.8	n^*=2
0	0.53213	0.71834	1.02619	1.41254	1.60394	2.22237	2.87975	3.99187
0.5	0.37868	0.58540	0.88693	1.29519	1.47926	2.11829	2.77871	3.90641
1	0.24746	0.46528	0.76853	1.18796	1.37278	2.02169	2.69045	3.8251
1.5	0.13174	0.35463	0.66442	1.08839	1.27876	1.93099	2.61121	3.74727
2	0.02764	0.25135	0.57085	0.994871	1.193927	1.84508	2.538793	3.672458

Table 5 — Heat transfer rate $-\theta'(0)$ for various values of Brownian motion parameter Nb^* and thermophoresis parameter Nt^*.

	$Nt^* = 0.3$		$Nt^* = 0.9$		$Nt^* = 1.5$		$Nt^* = 2$	
Nb^*	n^*=0.8	n^*=2	n^*=0.8	n^*=2	n^*=0.8	n^*=2	n^*=0.8	n^*=2
0.2	0.39898	0.54166	0.27473	0.40464	0.16702	0.28636	0.08946	0.20157
0.6	0.39898	0.54166	0.27473	0.40464	0.16702	0.28636	0.08946	0.20157
1.2	0.39898	0.54166	0.27473	0.40464	0.16702	0.28636	0.08946	0.20157
2	0.39898	0.54166	0.27473	0.40464	0.16702	0.28636	0.08946	0.20157

The impact of porosity parameter β^* on velocity is shown in Fig. 3. β^* has an inverse relationship with permeability K_p^* of porous media. A larger value of β^* causes stronger restriction to the fluid flow, which tends to slow down the fluid motion. Hence, the velocity of the fluid decreases with an increase of β^*. So we are sure that the result is consistent with the physics behind the concept of porosity.

Figure 4 shows the variation in $f'(\eta)$ with buoyancy parameter λ^*. Higher values of λ^* imply strong convection which tends to boost the flow velocity in the porous medium. Hence, velocity increases with increase in λ^*.

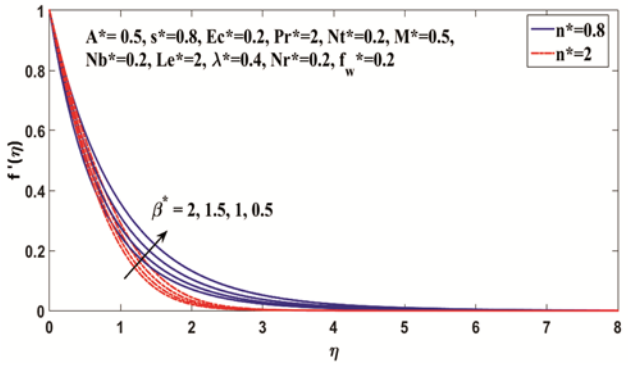

Fig. 3 — Behaviour of $f'(\eta)$ with β^* against η.

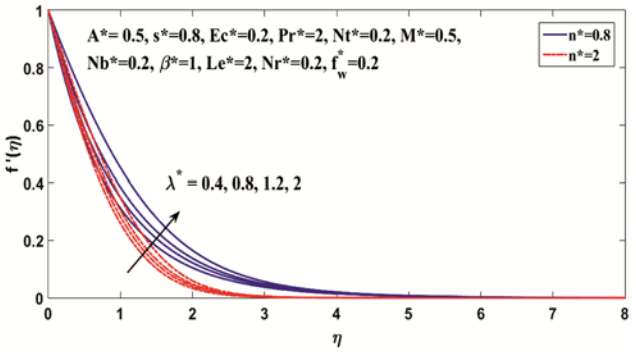

Fig. 4 — Behaviour of $f'(\eta)$ with λ^* against η.

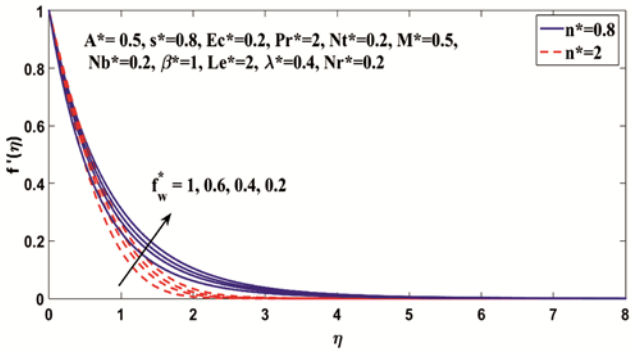

Fig. 5 — Behaviour of $\boldsymbol{f'(\eta)}$ with $\boldsymbol{f_w^*}$ against $\boldsymbol{\eta}$.

The impact of suction parameter f_w^* on $f'(\eta)$ is given by Fig. 5. A suction act to increase the cohesion of fluid to the surface which tends to retard the development of flow. Thus, with an increase in suction fluid velocity decreases.

The influence of physical parameters λ^*, β^*, $f_w{}^*$, and Br^* on the temperatureprofile is shown in Figs 6-9.

Figure 6 shows the behaviour of $\theta(\eta)$ against the buoyancy parameter λ^*. With the increase in the buoyancy parameter λ^* there is a decrease in the fluid temperature. So, higher values of λ^* corresponds to

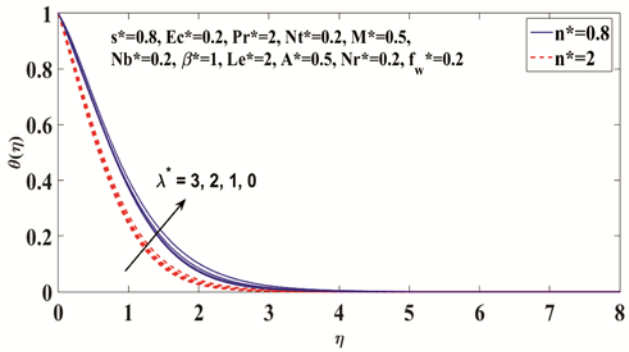

Fig. 6 — Behaviour of $\boldsymbol{\theta(\eta)}$ with $\boldsymbol{\lambda^*}$ against $\boldsymbol{\eta}$.

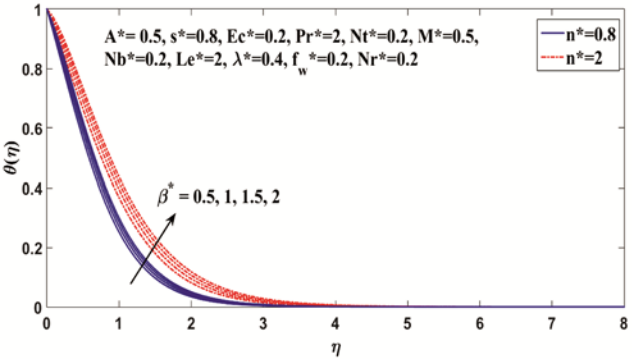

Fig. 7 — Behaviour of $\boldsymbol{\theta(\eta)}$ with $\boldsymbol{\beta^*}$against $\boldsymbol{\eta}$.

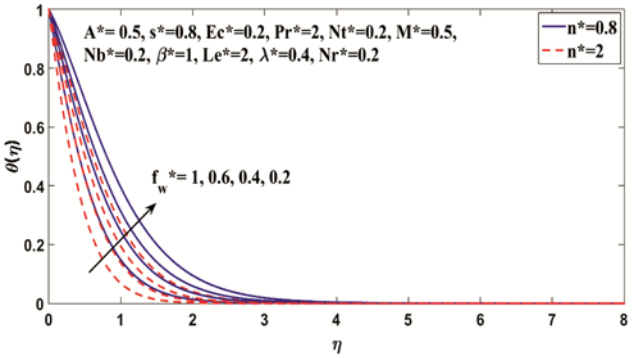

Fig. 8 — Behaviour of $\boldsymbol{\theta(\eta)}$ with $\boldsymbol{f_w^*}$ against $\boldsymbol{\eta}$.

the faster cooling of the stretching surface. Hence, the buoyancy parameter can be effectively used in many chemical and metallurgical processes to control the temperature.

The presence of solid particles in the medium increases with an increase in the porosity parameter β^*. This phenomenon decreases heat transfer, which tends to increase the temperature in a flow saturated porous regime. Hence, the temperature of fluid increase with an increase of β^* as given by Fig. 7.

Figure 8 depicts the behaviour of $\theta(\eta)$ with suction parameter f_w^*. The increasing values of suction parameter decreases the fluid temperature and hence suction can be used in industries for faster cooling of sheets.

The impact of Brinkman number Br^* on the temperature profile is shown in Fig. 9. Brinkman number is the ratio of heat generated by viscous dissipation to the heat transfer by molecular conduction. It signifies the heat conduction from the wall to the flowing fluid. Higher the values of Brinkman number Br^*, slower is the conduction and hence, larger will be the temperature. Hence, temperature increases with an increase of Br^*. For $Br^* \geq 1$, its found that temperature overshoot near the wall.

The variation in skin friction with buoyancy parameter λ^* for different values of suction f_w^* is shown in Figs 10-11 for both shear thickening $(n^* > 1)$ and shear thinning $(0 < n^* < 1)$ fluids. Increase in λ^* increases buoyancy forces which tends to enhance the velocity. Now, since the skin friction increase with an increase in velocity so skin friction will be larger for larger values of buoyancy parameter λ^*. From the figure, we can also conclude that skin friction decreases with increases in suction parameter f_w^* for both shear thinning and shear thickening fluids. Suction is applied to reduce the drag. The effect of suction is to stabilize the boundary layer and a reduction in drag is achieved by preventing the transition from laminar to turbulent flow[29].

Figures 12-13 show the variation in temperature and nanoparticle volume fraction with thermophoresis parameter Nt^*. Nt^* plays an important role in analyzing the temperature and nanoparticle volume

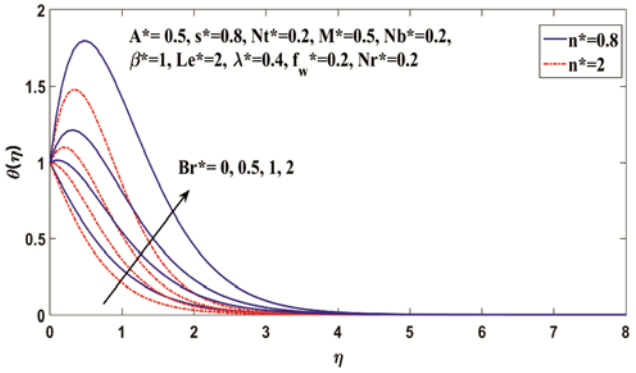

Fig. 9 — Behaviour of $\boldsymbol{\theta(\eta)}$ with $\mathbf{Br}^*$against $\boldsymbol{\eta}$.

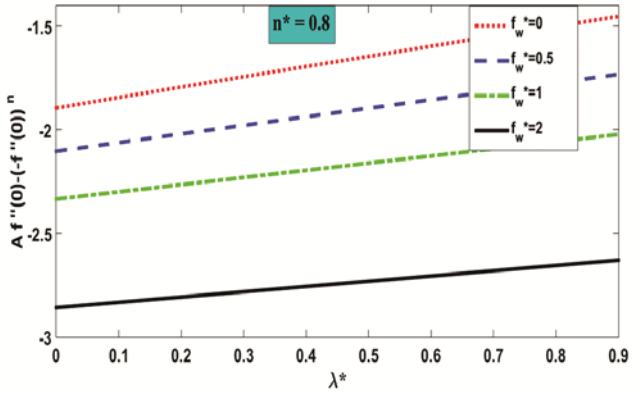

Fig. 10 — Variation in skin friction with f_w^* and λ^* for $n^* = 0.8$.

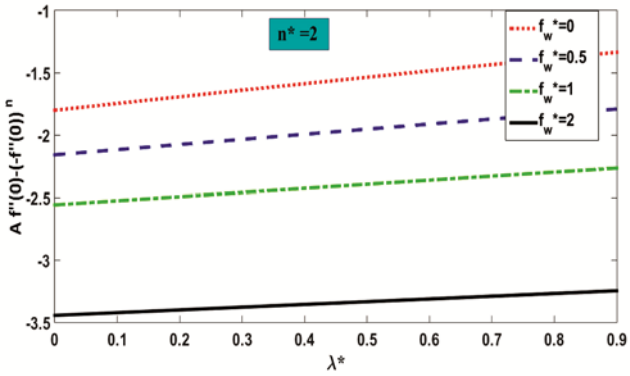

Fig. 11 — Variation in skin friction with f_w^* and λ^* for $n^* = 2$.

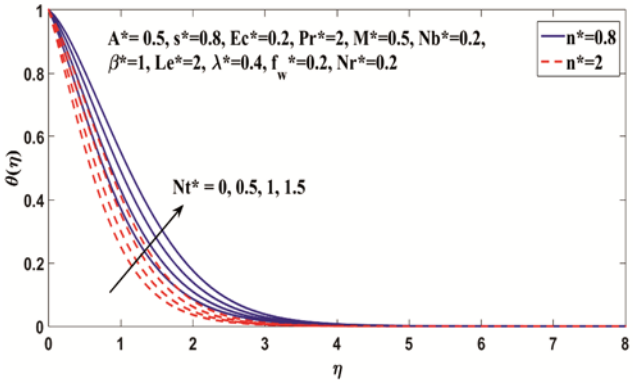

Fig. 12 — Behaviour of $\boldsymbol{\theta(\eta)}$ with $\boldsymbol{Nt}^*$ against $\boldsymbol{\eta}$.

fraction distribution in the nanofluid flow. Thermophoretic forces are produced due to larger values of Nt^* which migrates the nanoparticles in reverse direction of the temperature gradient. Hence, Nt^* increases the temperature and nanoparticle volume fraction.

Figures 14-17 give variation in the nanoparticle volume fraction $\phi(\eta)$ with physical parameters λ^*, β^* and Nb^* and Le^*. $\phi(\eta)$ has typical behaviour with η. Nanoparticle volume fraction firstly increases, then decreases and finally becomes zero with an increase in η.

The impact of the buoyancy parameter λ^* on the nanoparticle volume fraction is shown in Fig. 14. Higher values of the buoyancy parameter boost the buoyancy forces which results in increasing the mass transfer rate. Thus, nanoparticle volume fraction reduces with the enhancement of λ^*.

Figure 15 depicts the behaviour of $\phi(\eta)$ with porosity parameter β^*. The figure shows that nanoparticle volume fraction and corresponding boundary layer thickness increases with an increase in the porosity parameter β^*.

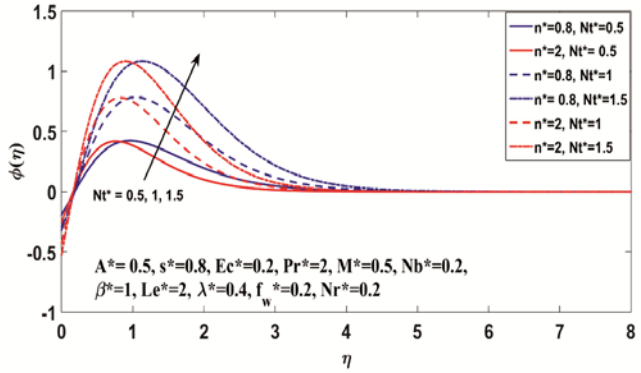

Fig. 13 — Behaviour of $\phi(\eta)$ with Nt^* against η.

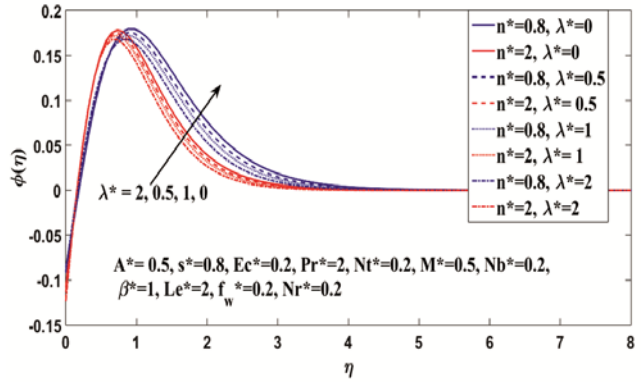

Fig. 14 — Behaviour of $\phi(\eta)$ with λ^* against η.

The impact of Brownian diffusion parameter Nb^* on $\phi(\eta)$ is shown in Fig. 16. With the increase in the value of Nb^* the random motion of the nanoparticle increases. A larger value of Brownian diffusion parameter Nb^* suppresses the diffusion of nanoparticle in a fluid regime which reduces the distribution of the nanoparticle volume fraction.

The influence of Lewis number Le^* on the nanoparticle volume fraction is shown in Fig. 17. For

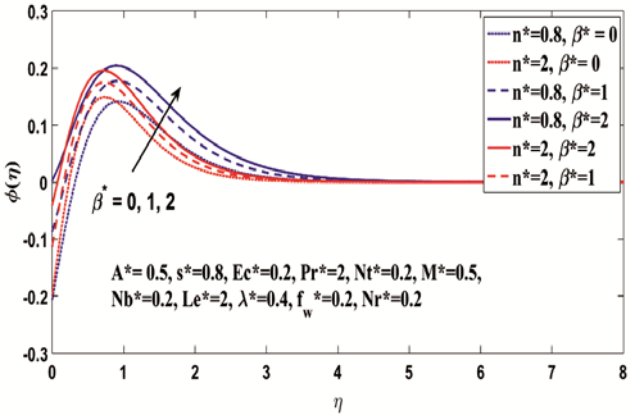

Fig. 15 — Behaviour of $\phi(\eta)$ with β^* against η.

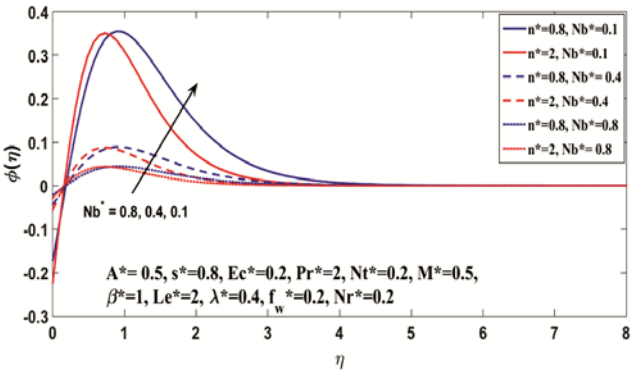

Fig. 16 — Behaviour of $\phi(\eta)$ with Nb^* against η.

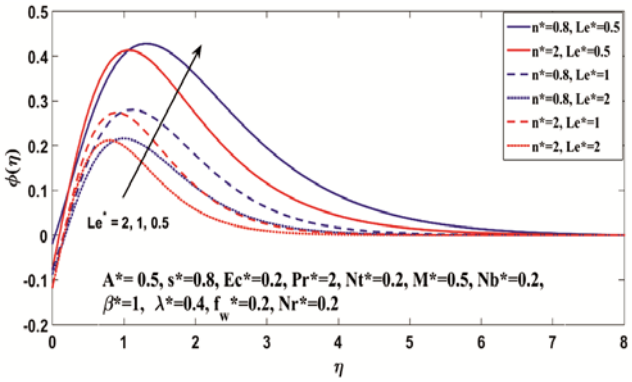

Fig. 17 — Behaviour of $\phi(\eta)$ with Le^* against η.

larger values of Le^* mass diffusivity decreases, which tends to decrease the nanoparticle volume fraction profile.

7 Conclusions

The main motive of this paper is to present the numerical solution for the flow and heat transfer of a magnetohydrodynamic Sisko nanofluid through a vertical stretching sheet in porous medium. Viscous dissipation effects are also taken into account. Moreover, zero nanoparticles mass flux condition is employed which leads to the passive control of nanoparticle fraction at the boundary. Using a suitable transformation, governing partial differential equations of fluid flow are transformed into a set of nonlinear ODEs. Numerical solutions are obtained using a finite difference technique in MATLAB software. The main findings of the above computations are as follows:

(i) The increasing values of the suction parameter f_w^* and porosity parameter β^* helps in reducing the skin friction at the wall,

(ii) Heat transfer rate enhances with f_w^* and diminishes with β^*. Thus, by the effective use of these parameters fast cooling of the stretching sheet can be achieved.

(iii) Porosity parameter β^* and Brinkman number Br^* heat up the porous regime. The fluid temperature increases with an increase in β^* and Br^* while it shows reverse behaviour with the f_w^* and λ^*. Hence, the fluid temperature can be modified to desired values by controlling these parameters,

(iv) Velocity profile increases with the increase in the Sisko material parameters A^* and buoyancy parameter λ^* while it reduces with suction parameter f_w^* and porosity parameter β^*, and

(v) Nanoparticle volume fraction increases with β^* while a reverse trend is observed for λ^*, Brownian motion parameter Nb^* and Lewis number Le^*.

Acknowledgment

Rajesh Sharma would like to acknowledge SERB, DST, Government of India for providing support for this work through research project (No. ECR/2016/000368). Ankita Bisht would like to thank the Ministry of Human Resource Development (MHRD), the Government of India and NIT Hamirpur for the grant of research fellowship.

References

1 Crane L, *Zeit Fur Angew Math Phy,* 21 (1970) 645.
2 Mahapatra T R & Gupta A S, *Heat Mass Transfer,* 38 (2002) 517.
3 Vajravelu K & Cannon J R, *Appl Math Comput,* 181 (2006) 609.
4 Cortell R, *Appl Math Comput,* 184 (2007) 864.
5 Gupta P S & Gupta A S, *Can J Chem Eng,* 55 (1977) 744.
6 Reddy R S & Sidawi G, *Appl Sci Res,* 52 (1994) 247.
7 Gupta A S, Misra J C & Reza M, *Fluid Dyn Res,* 32 (2003) 283.
8 Brinkman H C, *App Sci Res, A2* (1951) 120.
9 Nield D A, *Transport Porous Med,* 41 (2000) 349.
10 El-Amin M F & Ebrahim N A, *Transport Porous Med,* 64 (2006) 1.
11 Pal D & Hiremath P, *Meccanica,* 45 (2010) 415.
12 Al-Hadhrami A K, Elliott L & Ingham D B, *Transport Porous Med,* 53 (2003) 117.
13 Sharma R, *Appl Math Comput,* 219 (2012) 976.
14 Sharma R, Bhargava R & Bhargava P, *Comput Mater Sci,* 48 (2010) 537.
15 Ahmad S & Pop I, *Int Commun Heat Mass,* 37 (2010) 987.
16 Subhashini S V, Samuel N & Pop I, *Int Commun Heat Mass,* 38 (2011) 499.
17 Hayat T, Waqas M, Shehzad S A & Alsaedi A, *Scientia Iranica B,* 21 (2014) 682.
18 Hayat T, Waqas A, Shehzad S A & Alsaedi A, *Eur Phys J Plus*, 131 (2016) 253.
19 Waqas A, Shehzad S A, Hayat T, Ijaz Khan M & Alsaedi A, *J Phys Chem Solids,* 133 (2019) 45.
20 Waqas M, Farooq M, Khan M I, Alsaedi A, Hayat T & Yasmeen T, *Int J Heat Mass Transf*, 102 (2016) 766.
21 Waqas M, Khan M I, Hayat T, Gulzar M M & Alsaedi A, *Chaos, Solitons Fractals*, 130 (2020) 109415.
22 Choi S U S & Eastman J, *ASME-Publications-Fed,* 66 (1995) 99.
23 Buongiorno J, *ASME J Heat Transf,* 128 (2006) 240.
24 Sharma R, Ishak A & Pop I, *Indian J Pure Appl Phys,* 55 (2017) 275.
25 Sharma R & Bisht A, *AIP Conf Proc*, 1975 (2018) 030025.
26 Nayak M K, Shaw S & Makinde O D, *Indian J Pure Appl Phys,* 56 (2018) 773.
27 Hayat T, Waqas M, Shehzad S A & Alsaedi A, *J Mol Liq,* 222 (2016) 181.
28 Hayat T, Khalid H, Waqas M & Alsaedi A, *Comput Meth Appl Mech Eng*, 341 (2018) 397.
29 Afzal K & Aziz A, *Res Phys*, 6 (2016) 746.
30 Aziz A, Jamshed W & Aziz T, *Open Phys*, 16 (2018)123.
31 Hayat T, Waqas M, Shehzad S A & Alsaedi A, *J Mol Liq,* 223 (2016) 566.
32 Eid M R, Mahny K L, Muhammad T & Sheikholeslami M, *Res Phys,* 8 (2018) 1185.
33 Bisht A & Sharma R, *Int J Numer Meth Heat Fluid Flow*, (2019) https://doi.org/10.1108/HFF-08-2019-0629.
34 Waqas M, *J Magn Magn Mater*, 493 (2020) 165646.
35 Sisko A W, *Ind Eng Chem Res,* 50 (1958) 1789.

36 Eid M R & Mahny K L, *Heat Transfer-Asian Res,* 47 (2018) 54.
37 Doh D H, Muthtamilselvan M, Ramya E & Revathi P, *Commun Theor Phys,* 70 (2018) 230.
38 Soomro F A, Usman M, Haq R U & Wang W, *Int J Heat Mass Transf,* 126 (2018) 1034.
39 Ahmad L & Khan M, *Int J Hydrog Energy,* 44 (2019) 10197.
40 Sharma R & Bisht A, *AIP Conf Proc,* 2134 (2019) 030002.
41 Asghar Z, Ali N, Ahmed R, Waqas M & Khan W A, *Comput Meth Prog Bio,* 182 (2019) 105040.
42 Kuznetsov A V & Nield D A*, Int J Thermal Sci,* 77 (2014) 126.
43 Wang C Y, *J Appl Math Mech (ZAMM),* 69 (1989) 418.
44 Schlichting H & Gersten K, *Boundary layer theory*, (McGraw-Hill, New York), 7^{th} Edn, 2014.